PERIODICO di MINERALOGIA
established in 1930

DIPARTIMENTO
DI SCIENZE DELLA TERRA

SAPIENZA
UNIVERSITÀ DI ROMA

An International Journal of
Mineralogy, Crystallography, Geochemistry,
Ore Deposits, Petrology, Volcanology
and applied topics on Environment, Archaeometry and Cultural Heritage

An investigation on the zoning associated with divalent elements, P, Cr, Al and Ti in olivines from the Kilauea Iki lava lake (Hawaii)

Alessandro Fabbrizio *

Institute of Petrology and Structural Geology, Faculty of Science, Charles University, Albertov 6, 12843 Prague, Czech Republic

ARTICLE INFO

Submitted: January 2019
Accepted: March 2019
Available on line: April 2019

* Corresponding author:
alessandro.fabbrizio@natur.cuni.cz

DOI: 10.2451/2019PM845

How to cite this article:
Fabbrizio A. (2019)
Period. Mineral. 88, 185-201

ABSTRACT

The residual chemical zoning in olivine crystals can be used to reconstruct and decipher the history of a magma body. Olivine-bearing samples recovered from the drill KI81-1 of the Kilauea Iki lava lake have been investigated to interpret their zoning in divalent and trace elements. Divalent elements (Ni, Mn, and Ca) tend to be correlated to Fo contents, although no residual concentric chemical zoning is preserved for Ni, in response to the cooling of the magma body. Trace elements such as P, Ti, Al, and Cr are prone to develop skeletal enrichments as consequence of episodes of rapid crystal growth caused by the cooling of the lava lake itself. These observed features, coupled also with the absence of reverse zoning and of resorption features in olivine crystals, suggest that the Kilauea Iki lava lake could be viewed as approaching closely an ideal closed system.

Keywords: crystal; zoning; magma; temperature; cooling; growth.

INTRODUCTION

Kilauea Volcano erupted in November-December 1959 filling a pre-existing crater and forming a lava lake similar to a small magma chamber with a volume of approximately $40 \cdot 10^6$ m^3 (Murata and Richter, 1966; Richter et al., 1979; Wright, 1973; Helz, 1987a, 2009). After solidification and stabilization of the upper crust in December 1959, USGS has drilled repeatedly the lava lake from early 1960 to 1988 as it cooled and crystallized. Description of the drilling results are reported in full detail by Richter and Moore (1966) and by Helz (1987b, 1993). A simple geothermometer based on the wt% of MgO in the residual liquid (Helz and Thornber, 1987) enabled to place the thermal maximum in 1988 at a depth of 81.4 m, implying a total thickness of ~135 m in the center of the lake (Helz, 2009). In this study the residual zoning in olivine (phenocrysts and microphenocrysts) from samples recovered at different depths inside the lava lake during the drill KI81-1 in 1981 is investigated. Particular attention is given to the residual zoning of divalent elements (i.e., Fe/Mg, Ca, Mn, Ni), that are affected by linear cooling and by magma recharge or mixing, and of trace elements such as P, Cr, Al, and Ti, that are influenced by events of rapid crystallization (Bouvet de Maisonneuve et al., 2016).

During the last decade several studies have highlighted the potential use of chemical zoning in olivine for revealing related magmatic histories such as simple linear cooling, recharge and mixing events, as well as fast crystallization (Milman-Barris et al., 2008; Welsch et al., 2013, 2014; Bouvet de Maisonneuve et al., 2016; Neave et al., 2018; Jankovics et al., 2019). If a magma body was subject to a continuous and linear change of the intensive parameters (*P*, *T*, composition), minerals would be compositionally homogeneous or display simple zoning profiles, without reversal or discontinuities (Bouvet de Maisonneuve et al., 2016) and could be used as a tool to decipher with minimal ambiguity the magmatic process. If on one hand, in nature this scenario is extremely rare because in general

crystallization take places over a range of pressure and temperature, because of mixing of batches of magma with different composition, and because of interactions with wall rocks. On the other hand, the cooling and crystallization of a magma body erupted in a short time inside a pre-existing crater may approach closely the ideal situation. The studied samples reveal that: (i) olivine pheno- and micropheno-crysts can preserve, under some condition, zoning of divalent cations at magmatic temperatures; (ii) zoning in P, as shown by Milman-Barris et al. (2008), appears to be more resistant to diffusive relaxation; (iii) P is frequently associated with Al, Ti, and ±Cr. These features give to us information about early stages of olivine growth representing a potential archive of information on an otherwise inaccessible stage of magma's history. It is shown that combining info from zoning of divalent elements with those from P, Al, Ti, and ±Cr, and interpreting the residual P zoning preserved in the olivine crystals in light of the dendrite growth hypothesis (Welsch et al., 2013, 2014), a simple and linear crystallization history for the Iki lava lake can be drawn.

SAMPLES AND ANALYTICAL TECHNIQUES

Polished sections of olivine-bearing lavas were studied from the recovered drill core KI81-1 done by USGS at the Kilauea Iki lava lake (Hawaii) in 1981. For practical purpose the studied samples are subdivided as a function of their recovering depth as: shallow (from 45.3 to 60.3 m), intermediate (from 63.7 to 78.0 m), and deep (from 81.7 to 93.6 m). Thin sections were provided by the Smithsonian Institution. Information on these natural samples are given in Table 1. Representative images and analyses are shown, respectively, in Figure 1 and Table 2. Images of all samples are shown in Figure S1-S6 and the whole analytical data set is reported in the Deposited Item. Samples are identified by a number indicating their recovering depth in the lava lake, accompanied by the suffix indicating olivine grain or glass and in case of olivine by a lower case letter identifying the grain of interest (e.g., 66.4-Ol11b is referred to olivine 11, grain b in sample recovered from depth 66.4 m; 55.2-glass is referred to the glass from sample recovered from depth 55.2 m). I refer to microphenocrysts when grain size is <0.5 mm and if ≥0.5 mm to phenocrysts.

The K_a X-ray intensity maps of P, Al, Cr, Ti, Fe, Mg, Mn, Ni and Ca were obtained using the Jeol JXA-8200 electron microprobe at Caltech. The microprobe was used with an accelerating voltage of 15 kV, beam current of 400 nA, beam diameter of 1 mm (excitation volume ~1.4 microns across, calculated according to Potts, 1987), and pixel spacing of 1-3 mm in sessions lasting up to 93 hours. Beam current variations during map acquisition was ~1 nA. Maps for P, Cr, Al, Fe and Ti or Mg, Ni, Mn and Ca were acquired at the same time. The elements Ti and Mn were acquired on PETJ crystal, Fe on LIF, Cr and Ca on PETL, Al and Mg on TAP, P on PETH and Ni on LIFH. Dwell times of 120 ms were sufficient to detect zoning of divalent elements, whereas dwell times ranging from 420 to 1800 ms were needed to detect zoning in P, Cr and Al. Zoning in Ti was detected only using a dwell time of 1800 ms. Olivine grains (single spot analyses and/or quantitative line profiles across the zonation were done) and interstitial glass were analyzed for SiO_2, TiO_2, Al_2O_3, Cr_2O_3, FeO, MnO, MgO, CaO, NiO, Na_2O, K_2O, and P_2O_5. Routine or normal analysis conditions were: accelerating voltage 15 kV, beam current 40 nA for olivine and 10 nA for glass, beam diameter 1 μm for olivine and 10 μm for glass (5 μm for glass from sample 55.2). Counting times during olivine analyses were 80 s for P, 100 s for Cr and Al and 20 s for all the other elements, for glass analyses were 20 s (all elements). High precision analyses for olivine were done using a specialized setup to detect only trace element concentrations of P, Ti, Al and Cr with accelerating voltage of 15 kV, beam current of 400 nA and counting times of 200 s. These conditions were optimal to obtain good detection limits (in the range 9-15 μg/g). Standard used were: forsterite (Si in olivine; Mg in olivine and glass); VG2 basalt glass (Si in glass); rutile (Ti); anorthite (Al, Ca); chromite (Cr); fayalite (Fe); tephroite (Mn); albite (Na); Ni olivine (Ni); apatite (P); and K-feldspar (K). Data were reduced using a modified ZAF procedure (CITZAF; Armstrong, 1988). Secondary olivine (San Carlos and Guadalupe) and glass (BHVO-2g, BIR-1g, BCR-2g, and TB-1) standards were analyzed at the start and at the end of each microprobe session for a total of 6-10 points each. The mean compositions of the secondary glasses from each session coupled with their accepted compositions were used to correct all glass analyses from a session. Glass analyses were accepted if their post-correction totals were 100.0±1.5 wt%. The mean of SiO_2, MgO and FeO contents of secondary olivines from each session was compared with their accepted values to correct all olivine analyses from a session. The SiO_2 concentrations required no correction. Post-correction acceptance criteria for olivine included oxide sums of 100.0±1.5 wt% and cation sums of 3.000±0.015 per four oxygens and 1.000±0.015 Si+P cations per four oxygens.

RESULTS

Divalent elements

Zoning in divalent elements from X-ray maps

Major-element zoning (Figures 1, S6) is present in the shallow olivine phenocrysts and microphenocrysts. Generally, crystal cores are more forsteritic than rims. Zoning in Ca and Mn is present in olivine from depths 45.3 and 55.2 m. Here Ca behaves like Mg, whereas Mn shows

Table 1. Description of samples and presence of zonation for P, Cr, Al, and Ti as observed in X-ray maps.

Sample	Grain	Grain	zoning observed in X-ray maps[d]				Dwell time
ID[a]	ID[b]	type[c]	P	Cr	Al	Ti	(ms)
45.3-Ol1	a, b	Phn, Mphn	x	o	o	o	450
45.3-Ol2	c	Mphn	x	o	o	o	500
55.2-Ol3	a	Mphn	x	o	o	o	500
55.2-Ol4	b	Mphn	x	o	o	o	500
55.2-Ol5	c	Mphn	x	o	o	o	500
55.2-Ol5	c	Mphn	x	o	x	x	1800
57-Ol6	a	Mphn	x	o	x	o	700
60.3-Ol7	a, b, c, d	Phn	x	x	o	o	450
60.3-Ol8	e	Mphn	x	x	x	o	700
63.7-Ol9	a, b	Phn	x	o	o	o	1000
63.7-Ol10	c	Mphn	x	x	x	o	500
66.4-Ol11	a, b, c	Mphn	x	x	x	o	650
70.4-Ol12	a, b	Mphn	x	x	x	o	500
75.0-Ol13	a	Phn	x	x	x	o	420
75.0-Ol14	b, c	Mphn	x	x	x	o	900
75.0-Ol15	d	Mphn	x	x	x	o	1200
78.0-Ol16	a	Mphn	x	x	x	o	500
81.7-Ol17	a	Phn	x	x	x	o	1100
81.7-Ol18	b	Mphn	x	x	x	x	1500
83.8-Ol19	a, b, c, d	Mphn	x	x	o	o	900
83.8-Ol20	e	Mphn	x	o	o	o	500
83.8-Ol21	f	Mphn	x	o	o	o	500
83.8-Ol22	g, h, i	Mphn	x	o	o	o	500
86.9-Ol23	a	Phn	x	o	o	o	600
86.9-Ol24	b	Mphn	x	o	o	o	500
86.9-Ol25	c	Mphn	x	x	o	x	500
86.9-Ol26	d	Mphn	x	x	o	x	500
86.9-Ol27	e, f, g. h	Mphn	x	x	o	o	500
88.4-Ol28	a, b	Mphn	x	x	x	x	700
89.9-Ol29	a	Mphn	x	o	o	o	1100
89.9-Ol29	a	Mphn	x	x	x	x	1800
93.6-Ol30	a	Mphn	x	o	x	o	650

[a]Number indicates depth (m) inside the lava lake. [b]Letter indicates the grain of interest.
[c]Phn = phenocryst and Mphn = microphenocryst. [d]x = zoning of element is detected, o = zoning of element is not detected.

a reverse zoning. Normal Ca zoning is observed also in phenocrysts from depth 60.3 m whereas microphenocrysts from this depth and from depth 57.0 m are homogenous in Ca. Zoning in Ni was never observed. On the basis of the X-ray maps Olivine 63.7-Ol9b (Figure S6) shows the upper rim enriched in Mg, however this observation is not confirmed by the microprobe analyses (Deposited Item). Olivine rims show no evidence of reverse zoning.

Line profiles in divalent elements

Microprobe profiles (Figure 2) through olivines from shallow depth (45.3-60.3 m) confirm the zonation in divalent elements (i.e., Fe/Mg, Ca, and Mn) detected by X-ray maps. The line scans across crystals confirm that olivine from shallow depth are the strongest zoned with Fo content ranging from 75.5 (core) to 68.5 mol% (rim), CaO content decreasing toward the rims from 0.28 to 0.16 wt% and MnO content increasing from 0.26 wt% (core) to 0.39 wt% (rim). The inner parts (cores) of zoned

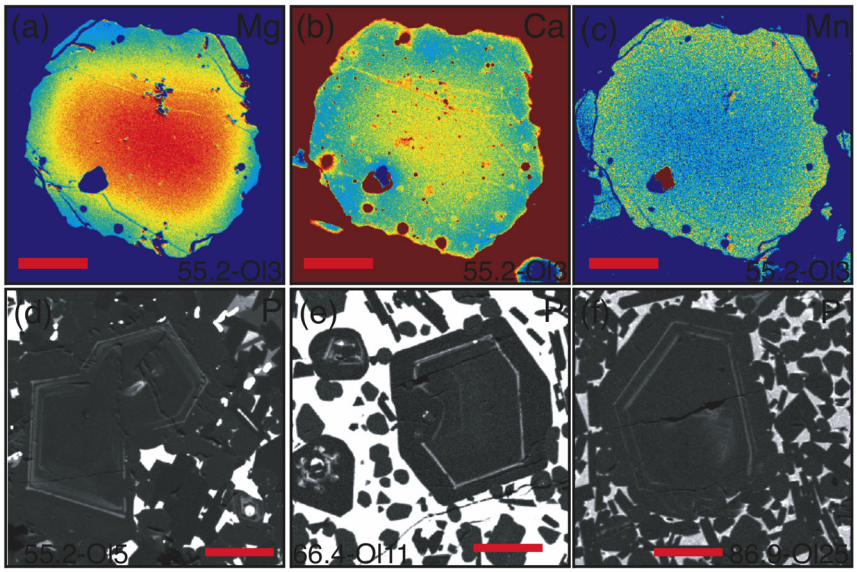

Figure 1. EPMA K_α X-ray intensity maps of Mg (a), Ca (b), Mn (c), and P (d-f) obtained from olivine crystals representative of the shallow (45.3-60.3 m), intermediate (63.7-78.0 m), and deep (81.7-93.6 m) portion of the Kilauea Iki lava lake. Olivine from the shallow portion is normally zoned in Mg (a), Ca (b), and inversely zoned in Mn (c). Similar P features are observed for olivine from shallow (d), intermediate (e), and deep (f) portion of the lava lake. See Figures S2, S3, S5 for additional details. Scale bars are 100 μm for all panels.

olivine have Fo content in the range 72.0-79.0 mol%. The cores display a relatively narrow range of CaO (0.25-0.28 wt%) and MnO (0.28-0.32 wt%) contents. The outer parts (rims) of zoned olivine have a more wide range of Fo content (68.5-78.5 mol%), CaO (0.16-0.25 wt%) but not in MnO (0.34-0.38 wt%). It also should be noted that no olivine is zoned in NiO, that olivine from intermediate depth to the bottom of the drill are unzoned in divalent elements and that the outermost rims of all crystals independently of their recovering depth are very enriched in CaO (up to ~1 wt%), also visible in the X-ray element maps for Ca as the brightest zones at the border olivine/matrix (Figure S6). These regions enriched in CaO are not related to the chemical zonation but they are an effect of secondary X-ray fluorescence of Ca (Dalton and Lane, 1996) from the adjoining Ca-rich phase (e.g., plagioclase, clinopyroxene, residual liquid). In conclusion, Fo, Ca, and Mn can be grouped together as already observed by Bouvet de Maisonneuve et al. (2016) given they display concentric zoning from core to rim being the normally zoning in Fo accompanied by positive zoning in Ca and negative zoning in Mn.

Trace elements

Zoning in P, Cr, Al, and Ti from X-ray maps

Zoning in P, based on X-ray intensity maps (Figures S1-S5), was observed in all examined olivines. Variations in P, Cr, Al, and Ti do not correlate with Fo. P fluctuations occur in the cores, close to melt inclusions, and at the rims both in pheno- and micro-crystals independently by their sampling depth. Fluctuations in Al and Cr occur mainly at the rims of the crystals, except for olivines 75.0-Ol14 and 75.0-Ol15, where they are observed at the center (Figure S3). The P zoning patterns of the olivines from the Iki lava lake are similar to those described by Milman-Barris et al. (2008), Welsch et al. (2013, 2014), Shea et al. (2015), Bouvet de Maisonneuve et al. (2016), Neave et al. (2018). The most common feature, observed both in phenocrysts and microphenocrysts, is an oscillatory zoning in P, sometimes accompanied by zoning in Cr-Al-Ti. Concentric P-rich bands parallel to the crystal edges, can occur as single band (e.g., Figure S1) or as two or more regularly spaced bands with similar or variable intensity along individual bands and/or from band to band near the outer edge of the crystal or anywhere inside the crystal (Figures S1-S5). Bands can be finely (5-20 μm), defining a fine-scale oscillatory zoning or widely spaced (e.g., tens of micron) forming concentric P-rich. All melt inclusions are enclosed in low-P regions cutting or disturbing the P-rich features (Figures S1-S3) similarly to the features described by Welsch et al. (2014), Bouvet de Maisonneuve et al. (2016), and Neave et al. (2018). The X-ray intensity maps for Cr, Al, and Ti show a weak or absent zonation for these element and consequently is difficult to find a spatial correlation with zonation in P. However, in some phenocrysts (Figure S1) zoning in P

Table 2. Representative analyses of olivine and coexisting glass (wt%).

Sample[a]	Grain ID	SiO_2	TiO_2	Al_2O_3	Cr_2O_3	FeO	MnO	MgO	CaO	NiO	Na_2O	K_2O	P_2O_5	Fo	Sum
55.2-Ol3	a	37.99	0.019	0.007	0.000	23.82	0.31	36.95	0.25	0.25	0.009	0.000	0.010	73	99.60
55.2-glass		70.14	2.14	16.07	0.025	5.83	0.05	1.67	3.11	0.03	0.03	0.07	1.15		100.33
57.0-Ol6	a	38.23	0.036	0.000	0.000	22.59	0.32	37.58	0.22	0.25	0.008	0.001	0.018	75	99.26
57.0-glass		57.00	3.21	13.82	0.000	8.78	0.16	3.31	6.02	0.00	4.17	2.29	1.11		99.88
60.3-Ol8	e	37.91	0.027	0.013	0.018	19.71	0.27	40.11	0.25	0.26	0.000	0.000	0.015	78	98.58
60.3-glass		53.07	4.82	13.20	0.013	11.20	0.17	5.47	9.35	0.00	0.19	0.97	0.52		98.97
63.7-Ol10	c	38.78	0.008	0.012	0.025	18.46	0.28	41.92	0.29	0.29	0.009	0.004	0.158	80	100.24
63.7-glass		51.19	3.99	13.09	0.018	10.53	0.11	5.99	9.86	0.00	2.89	0.88	0.40		98.94
66.4-Ol11	a	39.07	0.008	0.004	0.028	18.55	0.26	41.05	0.26	0.29	0.004	0.004	0.014	80	99.60
66.4-glass		50.85	3.61	13.43	0.014	11.21	0.15	6.08	10.06	0.00	2.74	0.86	0.40		99.42
70.4-Ol12	a	38.92	0.024	0.003	0.018	18.51	0.24	42.20	0.27	0.32	0.013	0.000	0.013	80	100.54
70.4-glass		51.20	3.93	13.42	0.049	11.47	0.16	5.63	10.00	0.00	2.95	0.87	0.43		100.11
75.0-Ol14	b	38.68	0.041	0.021	0.024	17.65	0.25	41.81	0.27	0.30	0.000	0.000	0.142	81	99.19
75.0-glass		52.26	3.99	13.54	0.043	10.51	0.16	6.29	10.08	0.02	0.91	0.89	0.45		99.16
78.0-Ol16	a	38.68	0.059	0.033	0.027	19.36	0.25	41.09	0.27	0.30	0.002	0.001	0.135	79	100.21
78.0-glass		53.16	4.14	13.59	0.033	11.50	0.18	6.07	10.15	0.04	0.13	0.91	0.47		100.36
81.7-Ol18	b	38.53	0.070	0.008	0.031	19.48	0.27	40.43	0.29	0.23	0.007	0.000	0.160	79	99.51
81.7-glass		50.94	4.33	12.95	0.022	11.61	0.21	5.77	9.61	0.00	3.20	1.00	0.49		100.14
83.8-Ol19	a	38.43	0.023	0.009	0.004	22.82	0.33	39.05	0.27	0.23	0.000	0.000	0.040	75	101.20
83.8-glass		50.50	4.16	12.10	0.000	14.54	0.22	5.19	9.12	0.00	2.70	0.87	0.47		99.89
86.9-Ol24	b	38.69	0.031	0.082	0.015	20.33	0.30	39.96	0.25	0.27	0.000	0.000	0.166	78	100.09
86.9-glass		50.90	5.08	11.98	0.013	12.36	0.18	5.45	8.57	0.00	2.85	1.12	0.53		99.04
88.4-Ol28	a	38.61	0.018	0.003	0.011	21.45	0.29	39.51	0.23	0.29	0.015	0.000	0.015	77	100.44
88.4-glass		51.63	5.27	12.68	0.003	12.14	0.18	4.89	8.45	0.02	3.09	1.17	0.60		100.13
89.9-Ol29	a	38.53	0.030	0.005	0.000	21.26	0.32	40.09	0.22	0.23	0.013	0.000	0.082	77	100.79
89.9-glass		56.47	4.45	13.05	0.007	10.42	0.22	4.86	7.87	0.01	0.26	0.68	0.85		99.16
93.6-Ol30	a	38.04	0.010	0.011	0.000	23.20	0.32	37.36	0.20	0.24	0.013	0.001	0.050	74	99.44
93.6-glass		58.54	3.63	14.32	0.006	10.47	0.13	4.02	7.23	0.00	0.13	0.32	1.09		99.90

[a]See Table 1 for additional information on samples.

is strongly coupled spatially with that of Cr and Al. In addition phenocryts 81.7-Ol17a (Figure S1) shows a wider band for Cr and Al respect to the P band. All other phenocrysts show no zoning in Cr and Al. Ti zoning was never detected in phenocrysts. In the microphenocryts 55.2-Ol5c (Figure S2) and 89.9-Ol29a (Figure S5) P, Cr, Al and Ti zoning are detected (Cr zoning undetectable in olivine 55.2-Ol5c) when using a dwell time of 1800 ms (Table 1), however zoning in Cr, Al, and Ti are really faint. Nevertheless in these olivines Cr, Al, and Ti zoning tend to spatially correlate with the high-P zones at the rims. In microphenocryst 60.3-Ol8e P, Al, and Cr seems to be correlated but the boundaries of the high-Cr region are more diffuse than the same boundaries in P and Al, and zoning in Al is extremely faint (Figure S3). Most of the microphenocrysts (e.g., Figures S3-S5) show strong zoning in P, weak zoning in Cr, and extremely weak zoning in Al. In still other microphenocrysts (e.g., Figure S3) Cr and Al zoning are enhanced by the presence of submicrometric (<1 μm) grains of chromite laid along the P-rich bands. In microphenocryts from depth 83.8 m no detectable features were observed in the X-ray maps for any element was measured. Microphenocryst 93.6-Ol30a shows zoning in P (Figure S5) but zoning in Al is faint and that in Cr in undetectable. It is also important to note that a lack of observable zoning on an X-ray map does not mean the absence of an element: in particular, as shown in the high definition profiles across P zonation, concentrations of Cr, Al and Ti are almost always above background and detection limit.

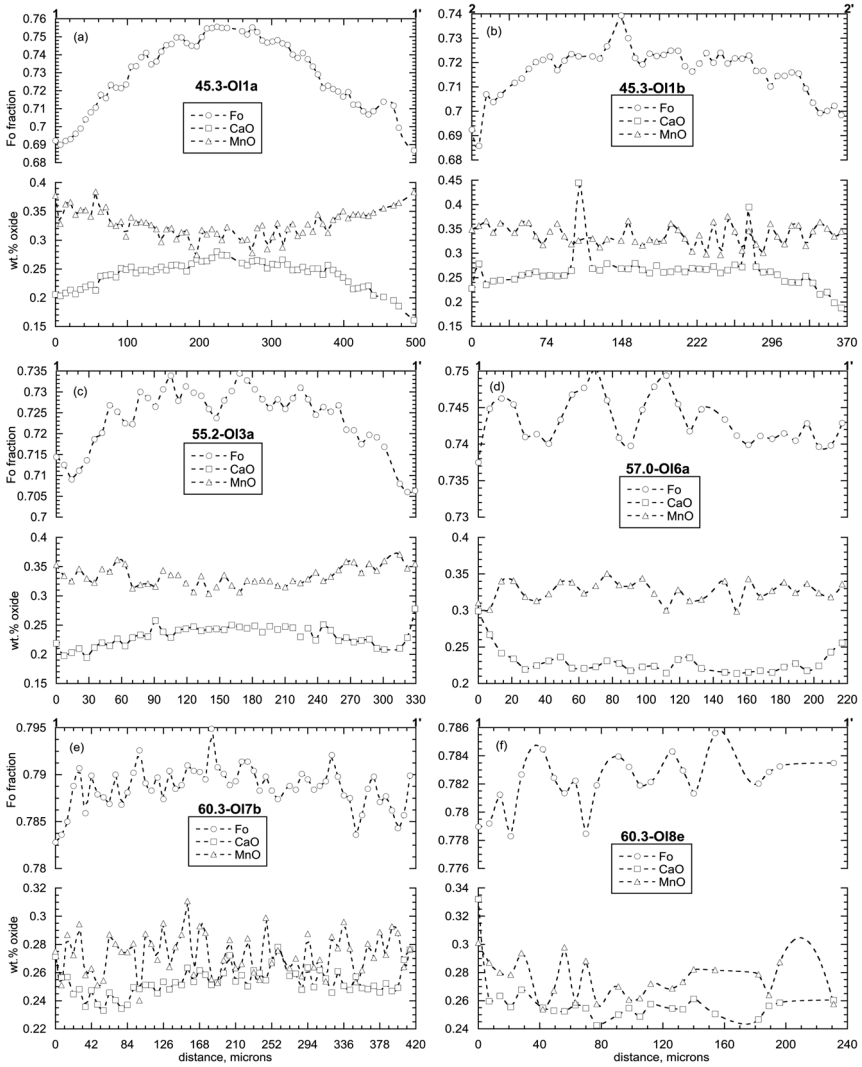

Figure 2. Microprobe quantitative profiles across olivine crystals (a-f) for Fo (circles), CaO (squares) and MnO (triangles). Numbers 1-1' or 2-2' indicate the direction of the profiles as shown in Figure S6.

High Definition profiles across P zoning

Many high definition (HD) line analyses across P zonation in most of the samples were performed to understand the potential relationships between trace elements (i.e., P, Cr, Al, and Ti) in olivines from different depths inside the lava lake. Extracts of the profiles are presented in Figure 3 and a full comment of each profile is given in the figure caption. Concentration in P_2O_5 ranges from 0.005 to ~0.19 wt% (detection limit 11-13 μg/g), TiO_2 varies between ~0.02 and ~0.084 wt% (detection limit 16-17 μg/g), Cr_2O_3 changes from below the detection limit (9 μg/g) to a maximum value of 0.074 wt %, and Al_2O_3 is from below the detection limit (14-18 μg/g) to ~0.105 wt%. All the profiles confirm the presence of the zonation in P having found a spatial correspondence between the high-P bands observed in the X-ray maps and the high definition line scans and most of them show the presence of TiO_2 and Al_2O_3, not always detected in the X-ray maps, related to P_2O_5, whereas only few samples show a detectable Cr_2O_3 content related to P_2O_5 peak. The profiles show that the analyzed P-bands are 3-10 μm wide with a symmetric (55.2-Ol5c, 57.0-Ol6a, 75.0-Ol14c, 81.7-Ol17a, 88.4-Ol28a, 89.9-Ol29a) or a little bit asymmetric sharp peak (45.3-Ol2c, 66.4-Ol11a, 75.0-Ol13a, 81.7-Ol18b, 86.9-Ol25c), few samples (55.2-Ol5c, 81.7-Ol17a, 93.6-Ol30a) show a more rounded high-P peak. When detected, peaks in Cr_2O_3, Al_2O_3, and TiO_2 tend to follow the shape and the position of the P_2O_5-peak. However, in sample 66.4-Ol11a, Al_2O_3 seems to be better correlated with TiO_2 and Cr_2O_3 with P_2O_5.

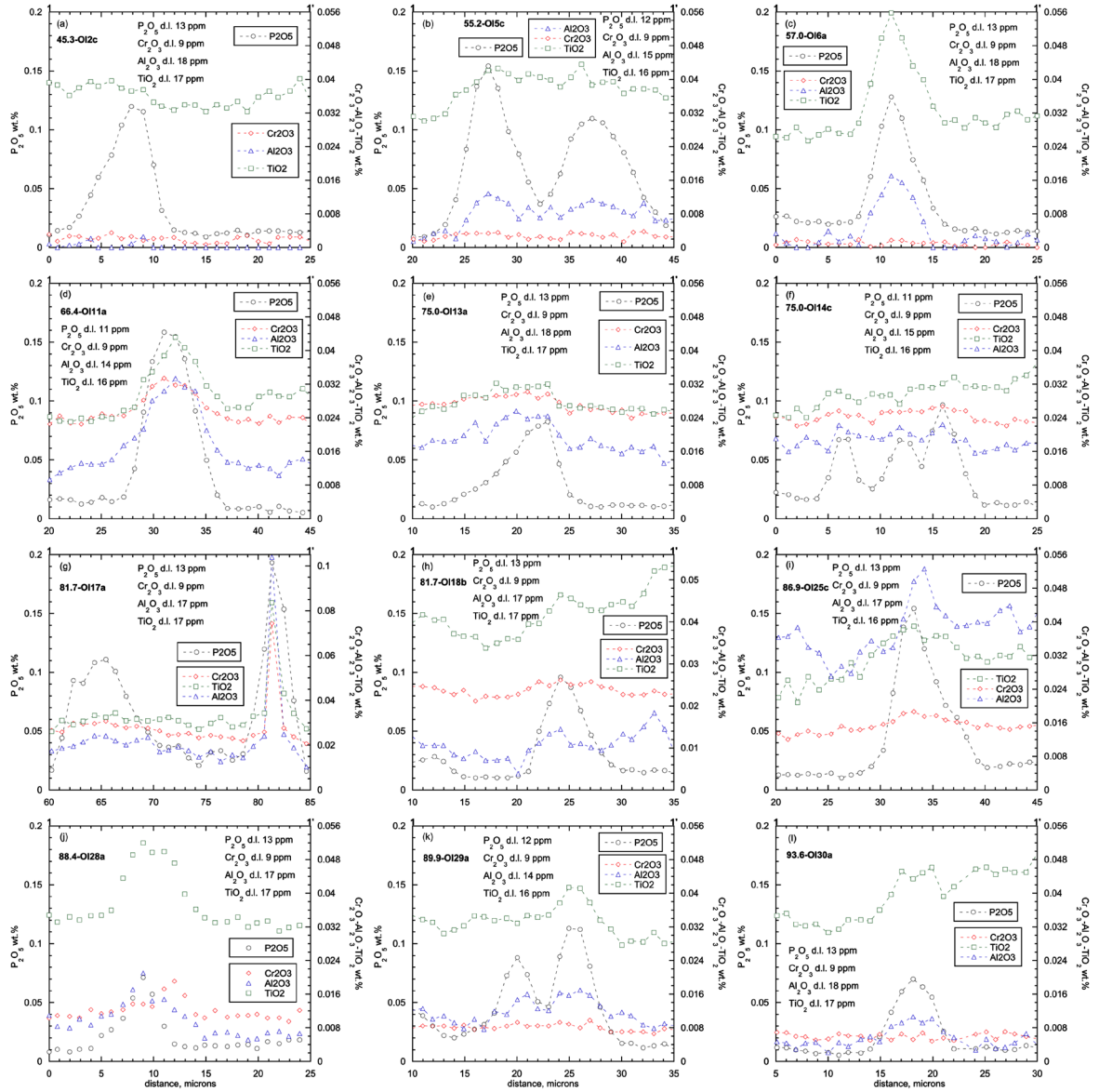

Figure 3. High-definition profiles across olivine zonation for phosphorus (open circles), chromium (open diamonds), aluminum (open triangles), and titanium (open squares). Numbers 1-1' indicate the direction of profile as shown in Figures S1-S5. (a), 45.3-Ol2c, it displays only a phosphorus peak; (b), 55.2-Ol5c, it has P_2O_5 spatially related with Al_2O_3; (c), 57.0-Ol6a, it is characterized by a well defined and sharp phosphorus-aluminum-titanium peak; (d), 66.4-Ol11a, a clear peak is detected for all the element of interest, in this case it seems that aluminum is spatially coincident with titanium and chromium with phosphorus; (e), 75.0-Ol13a, it shows an asymmetric peak for P_2O_5 related to a 5 µm wide region slightly enriched in Cr_2O_3, Al_2O_3, and TiO_2 respect to their background levels; (f), 75.0-Ol14c, three high-P peaks are visible (at the distances 6, 12, and 16 µm), chromium, aluminum, and titanium seems to have a peak value coincident wit phosphorus but their concentration do not change so much respect to the background level; (g), 81.7-Ol17a, it has two features: (i) on the left side of the graph a wide phosphorus-rich region is visible (62-67 µm), inside this region the other element of interest show a light enrichment, (ii) on the right side of the graph a very sharp P-Cr-Al-Ti peak is detected having anomalous high Cr-Al-Ti contents, may be this peak is related to the presence of a micrometric melt inclusion below the olivine surface; (h), 81.7-Ol18b, it shows a P_2O_5 peak at 24 µm related with Al_2O_3, and TiO_2, Cr_2O_3 display a relaxed region (located at 22-27 µm) slightly Cr-rich respect to its background level; (i), 86.9-Ol25c, it has a well defined P_2O_5 peak related to Al_2O_3 and TiO_2 content, aluminum and phosphorus increase abruptly from the background concentration in correspondence of the peak value whereas titanium shows a more gently increase, also chromium shows a very light peak at the position 33 µm as suggested by the interpretation of Cr X-ray map; (j), 88.4-Ol28a, it has well defined P-Cr-Al-Ti peaks, the Cr peak is not perfectly coincident with the P-Al-Ti peaks; (k), 89.9-Ol29a, it is characterized by a coincident peak for phosporus, aluminum, and titanium, no peaks for chromium are displayed; (l), 93.6-Ol30a, it has P_2O_5, Al_2O_3, and TiO_2 peaks spatially related between them, no peaks for Cr_2O_3 are detected.

The HD profiles are giving the following information: (i) they confirm that the shallowest olivine (45.3-Ol2c) has no zonation in Cr, Al and Ti; (ii) they reveal in most of the olivines the presence of a zonation in Ti that was not detected by the X-ray maps except for the map done at the highest dwell time (1800 ms) and that the background content of TiO_2 (~0.03 wt%) in olivine is almost constant with depth; (iii) show that relatively high Al_2O_3 contents were detected in all samples (except 45.3-Ol2c) in association with high P_2O_5 contents, and that Al_2O_3 background concentrations change from below the detection limit for the shallowest olivine to ~0.01 wt% at intermediate depth, reaching a value of ~0.035 wt% at a depth of 86.9 m and decreasing to below 0.008 wt% in the deepest sample; (iv) suggest that Cr zonation is the more prone to be dissolved not having observed a well defined Cr-peak well away from its background except in samples 66.4-Ol11a, 81.7-Ol17a and 88.4-Ol28a, background Cr_2O_3 concentrations are comparable to Al_2O_3 background contents being ~0.002 wt% in the shallowest samples, ~0.024 wt% in the intermediate samples and then progressively moving down to 0.008 wt% in the deepest ones. From the description above, P, Al, Cr, and Ti can be grouped together given they are not correlated with Fo and display concentric or skeletal enrichments in the olivine crystals.

Glass composition

Microprobe analyses of interstitial glass were made for all analyzed samples, except the sample recovered from depth 45.3 m given it has no residual glass. Table 2 reports selected glass analyses whereas the full data set is presented in the Deposited Item. Figure 4 shows average concentrations of oxides from the natural glasses as a function of depth. Concentration of SiO_2 decreases from 72.5 (55.2 m) to 50.5 wt% at a depth of 66.4 m; between 66.4-88.4 m it remains constant, until it increases up to 57 wt% in the deepest sample (93.6 m). Al_2O_3 shows similar trend, whereas FeO behaves oppositely with respect to SiO_2. MgO and CaO are typified by an "arcuate" trend,

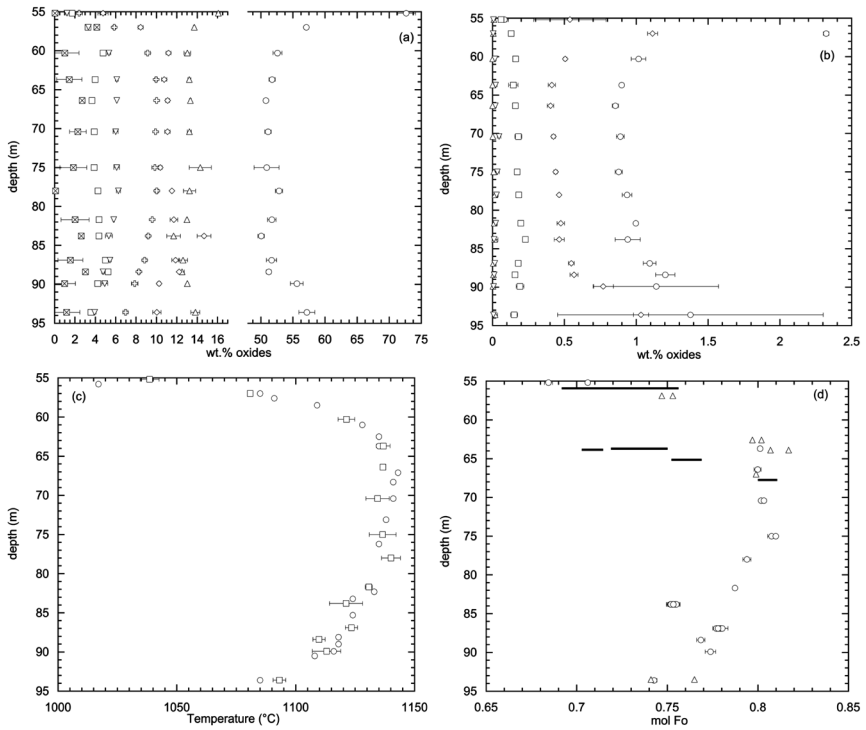

Figure 4. (a), variation of residual melt composition (wt%), major elements, for the Iki lava lake samples with recovering depth (m). Open circles, SiO_2; open triangles Al_2O_3; open diamonds, FeO; open crosses, CaO; reverse triangles, MgO; open squares, TiO_2; crossed squares, Na_2O. (b), variation of residual melt composition (wt% for K_2O, P_2O_5, MnO, NiO, and Cr_2O_3), for the Iki lava lake samples with recovering depth (m). Open circles, K_2O; open diamonds, P_2O_5; open squares, MnO; triangles, NiO; reverse triangles, Cr_2O_3. (c), liquid temperatures (°C) as function of depth (m) calculated by means of the empirical geothermometer of Helz and Thornber (1987). Open circles, original data from Helz and Thornber (1987); open squares, quenching temperature calculated using the wt% of MgO in the liquid. (d), variation of the Fo content in Iki olivine (microphenocrysts) with depth inside the lake. Open circles, data from this study; open triangles, data from Teng et al. (2008). Two types of data are shown: (i) average of multiple analyses in the core of the olivine crystal (open circles), and (ii) variation min-max Fo content inside the crystal of interest (black heaviest lines).

reaching the highest concentration (respectively 6.3 and 10 wt%) at a depth of 78.0 m. K_2O and P_2O_5 behave similarly to SiO_2. Na_2O and TiO_2 concentration do not show any particular correlation with depth. Cr_2O_3 and NiO contents are always below 0.05 wt%.

Temperature profiles versus depth

Helz and Thornber (1987) determined the variations of MgO contents of glasses as function of the temperature in melting experiments on appropriate Kilauean samples for use as an empirical geothermometer directly applicable to interstitial glasses in olivine-bearing core from Kilauea Iki. These authors demonstrated that glass geothermometry provides the greatest detail on temperature profiles in the partially molten zone, much of which is otherwise inaccessible, and permits the construction of a complete temperature profile for any given drill hole.

In Figure 4 the temperature estimates derived from glass compositions using the equation T (°C)=20.1$(MgO_{wt\%})^{liq}$ +1014 °C (Helz and Thornber, 1987), are compared with the original estimates from Helz and Thornber (1987). Samples recovered from the shallow portion of the lava lake show the largest temperature variation being in the range 1038-1121 °C, with temperatures increasing positively with depth at a rate of 16.3 °C/m. The intermediate portion registers a quite uniform temperature profile with a temperature variation in the range 1134-1140 °C and the maximal temperature located at a depth of 78.0 m. The deep portion is characterized by a decreasing temperature, from 1131 to 1093 °C, with increasing depth at an approximate rate of 3.2 °C/m. In general, considering that the uncertainty for temperature estimates for the original data of Helz and Thornber (1987) is ±8-10 °C, the temperature profile versus depth produced by the new data is well in agreement with the results of Helz and Thornber (1987) both in terms of the absolute values for the calculated temperatures and of the temperature variation as a function of depth.

Relationship between depth and olivine content

Forsteritic content of olivine microphenocryts positively correlates with the temperature variation inside the lava lake (Figure 4). An exception is represented by olivine microphenocryts from depth 83.8 m, which are less magnesian (Fo_{75}) than what expected by temperature values obtained by the Helz and Thornber (1987) thermometer (~1120 °C; i.e., ~Fo_{78}). This discrepancy could be explained by the presence of plagioclase inclusions, as shown in Figure S4 samples 83.8-Ol19-22, lowering thus the Fo content of the hosting olivine. Only few data relating Fo content in olivine with depth from the study of Teng et al. (2008) are available. In general both data sets show that olivines becomes progressively more Fe-rich as the temperature decreases and show more scatter in the lower-temperature samples, reflecting partial reequilibration of olivines with evolving residual melts (Teng et al., 2008).

DISCUSSION

Implications for magmatic processes at the Iki lava lake

Compositional zoning in olivine provides information about the dominant magmatic processes occurred in the Iki lava lake. These processes should leave a particular fingerprints in olivine crystals, and more in general in any associated crystal, that will be reflected in different zoning patterns for elements following Fo (i.e., Ca and Mn) and for those following P (i.e., Al, Cr, Ti). The interpretation of olivine zoning can help us to shed a light on the probable magmatic events characterizing the Iki lava lake, such as (1) filling of the crater by mafic magma eruption; (2) degassing and crystallization at low pressure of the magma body; and (3) absence of subsequent recharge events.

Relationship among Ca, Mn, Ni and Fo

The major and trace elements zoning can be attributed to variations in temperature as the magma body of the lava lake looses its heat and cools down. The absence of reversely zoned olivines is interpreted as the result of the cooling of the magma body without replenishment of more mafic and hotter magma. The strong correlations between Fo contents and abundances of Ca, Mn, and Ni suggest that their concentrations are also controlled by magma composition and hence by his temperature.

Positive correlation between Fo contents and Ni (Figure 5) is consistent with distribution coefficient values, $K_{Ni}^{ol/liq}$, greater than unity (Dostal et al., 1983; Villemant, 1988; Matzen et al., 2013, 2017; Bouvet de Maisonneuve et al., 2016). Being a compatible element Ni is favourably incorporated in olivines crystallizing from the less evolved silicate liquids and consequently depleted in the more evolved residual liquids from which more evolved olivines crystallize.

Also Mn in olivines should be positively correlated with their Fo contents given its compatibility, $K_{Mn}^{ol/liq}>1$, as reported by Watson (1977) and Gaetani and Grove (1997). However, Mn concentrations are negatively correlated with Fo contents (Figure 5) as it would be an incompatible element. This apparent opposite behavior can be explained considering the ionic radius (Shannon, 1976) of Mg^{2+} (0.72 Å), Fe^{2+} (0.78 Å), Mn^{2+} (0.83 Å) and the size of the six-fold octahedral site being more close to that of Mg^{2+} or Fe^{2+} rather than that of Mn^{2+} (Blundy and Wood, 2003). Because of its bigger ionic radius, Mn is rejected by Fo-rich olivine in favour of Mg and Fe, and it accumulates in the residual liquid, as testified by the Mn enrichment in the more evolved (Fo-poor) olivines.

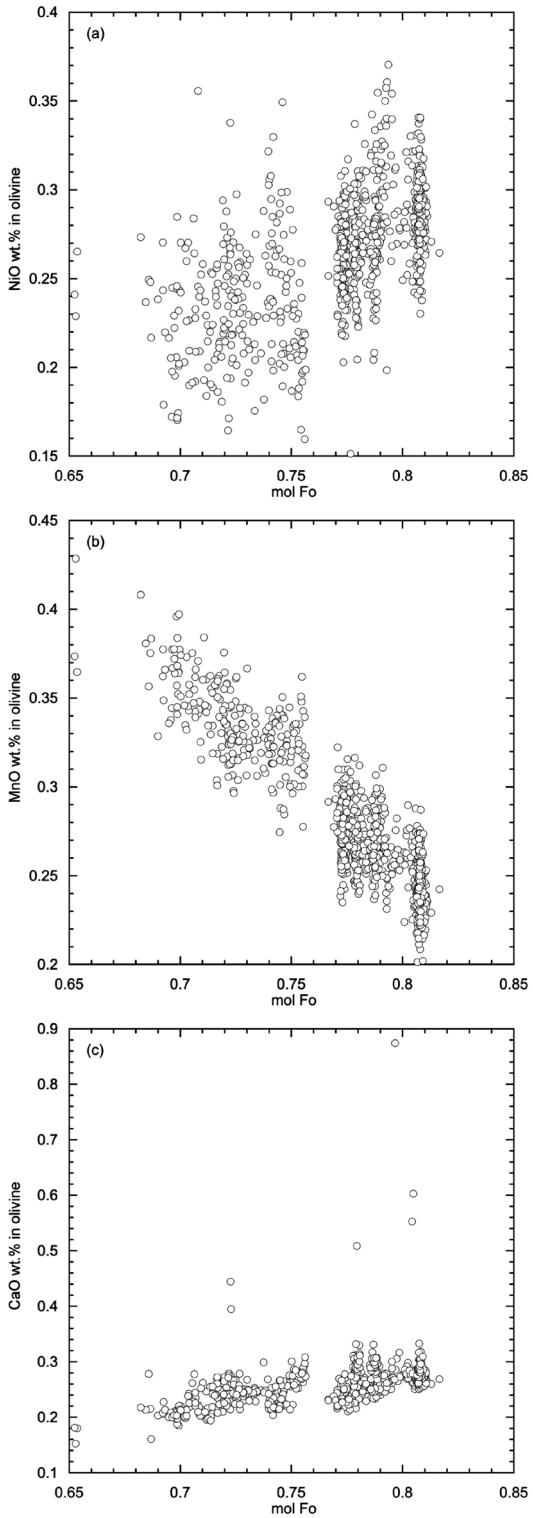

Figure 5. (a), NiO; (b), MnO; (c), CaO concentrations as a function of Fo content in the olivines of the Iki lava lake. All analyzed points are reported; i.e., oxide concentrations from line traverses and single spots. The highest CaO concentrations (>0.4 wt%) are due to X-ray fluorescence contamination from Ca-bearing phases (i.e., plagioclase, clinopyroxene, melt).

Given that Ca behaves as an incompatible element (Dunn, 1987; Beattie, 1994) it should be enriched in the melt as it crystallizes, and a negative correlation with Fo contents should be found. However, Ca concentrations are positively correlated with Fo contents (Figure 5). This second discrepancy can be understood considering that olivine does not crystallize alone in the Iki lava lake but it is accompanied by the crystallization of Ca-bearing mineral phases such as plagioclase and clinopyroxene. The contemporaneous crystallization of plagioclase and clinopyroxene depletes the residual melt in Ca and the more evolved liquids are poorer in Ca respect to the less evolved ones given that Ca is a compatible element in these mineral phases. As a result the more evolved olivine compositions display lower Ca contents respect to the less evolved ones.

The linear patterns defined by Fo contents and Ca, Mn, and Ni concentrations can be interpreted as representing the cooling and crystallization of the magma body in the lava lake without no recharge event. However, other elements such as P, Ti, Al, and Cr may provide additional information on magmatic processes.

Relationship between zonation in P, Cr, Al, Ti

X-ray maps (Figures S1-S6) show that zoning in phosphorus appears to be independent from zoning of divalent elements and that is difficult to spatially relate zoning in P with that of Al, Cr, and Ti because Al- and Cr-rich regions are wider (i.e., more diffuse) than the same regions in P (Figures S1, S3) or because zoning in Al-Cr-Ti is faint or undetectable (e.g., see and compare the two X-ray maps in Figure S2 obtained on the same crystal with different acquisition time) may be due to the low concentration of the element of interest (e.g., Cr) or to the extremely high acquisition time needed to detect them (e.g., Ti). The quantitative HD profiles across P zonation seems to be the best way to obtain information regarding spatial relationship for P-Cr-Al-Ti zonation.

The high definition profiles (Figure 3) indicate P-Al-Ti correlation sometimes associated with that of Cr. Previous works (Milman-Barris et al., 2008; Edmunson et al., 2005; Neave et al., 2018) found an association of P with Cr and/or Al but not with Ti (except only experiment 1 of Milman-Barris et al., 2008). The presence of Ti peaks related to P zoning in most of the investigated microphenocrysts (see Figure 3) confirm that Ti is hosted in the tetrahedral site as P by direct substitution with Si (Berry et al., 2007). The HD profiles reported in Figure 3 display strong correlations among P-Ti-Al and sometimes Cr for olivine microphenocrysts recovered at different depth inside the Iki lava lake. These microphenocrysts have experienced high temperatures (~1040-1140 °C cfr. Figure 4) for a relatively short residence time (~22 years, i.e., the time

difference between the time of drilling in 1981 and the time of eruption in 1959) and consequently as shown by Milman-Barris et al. (2008) the interrelationships between P-Ti-Al-Cr are evidence of rapidly grown igneous olivine. The absence of clear Cr-peak in most of the Iki crystals could suggest that Cr diffuse faster than Al in contrast with the experimental results and natural evidences of Milman-Barris et al. (2008), however three different reasons could explain the absence of Cr-peak associated with P zoning and solve this apparent discrepancy. (i) Iki olivine microphenocrysts are characterized by extremely low amount of Cr_2O_3, from below detection limit to up 0.032 wt%, these Cr_2O_3 concentrations are 4-7 times lower than the corresponding concentrations from the experiments of Milman-Barris et al. (2008) and ~3 times lower than Cr_2O_3 content from other Hawaiian olivines (Milman-Barris et al., 2008). The low Cr_2O_3 concentration in the Iki olivine is a reflection of the low Cr_2O_3 availability in the corresponding residual glass (ranging from below 0.01 to 0.05 wt%, see glass analyses in the Deposited Item). Roeder and Reynolds (1991) demonstrated that the Cr_2O_3 content of basaltic melts saturated with chromite at an fO_2 near the QFM buffer decreases from 0.12 wt% at 1300 °C to 0.05 wt% at 1200 °C. Scowen et al. (1991), comparing the Cr content of glass in Kilauea Iki pumices with those of a series of glasses quenched from the Kilauea Iki lava lake, found that Cr_2O_3 content of the glasses ranged from ~0.07 wt% at 1200 °C to <0.01 wt% at 1100 °C. The geothermometer of Helz and Thornber (1987) gives glass temperatures in the range 1040-1140 °C (Figure 4) and consequently the glasses from the Iki lava lake are characterized by lower Cr_2O_3 content respect to the experimental glasses obtained at 1200 °C by Milman-Barris et al. (2008). (ii) The zoning in Cr is weak or absent in natural olivines from the Iki lava lake because they were exposed at magmatic temperatures for longer time, ~22 years, if compared with the short duration of experimental runs, less than 20 hours (Milman-Barris et al., 2008). (iii) Many authors studying Hawaiian lavas suggest redox conditions close to the QFM buffer (Byers at al., 1985; Carmichael, 1991; Poustovetov and Roeder, 2001; Roeder et al., 2003; Rhodes and Vollinger, 2005), implying that most of Cr should be present as Cr^{3+}. However, Berry and O'Neill (2004) and Berry et al. (2006) demonstrated that Cr^{2+} is an important and possibly dominant oxidation state in basaltic volcanism at terrestrial fO_2 values. Moreover, Carmichael and Ghiorso (1986) noticed that some submarine Kilauea lavas are more oxidized than many subaerial Kilauea lavas, suggesting that the subaerial lavas become reduced during eruption due to the degassing of sulfur. It should be noted that most of the natural Hawaiian olivine crystals investigated by Milman-Barris et al. (2008) characterized by a well developed and prominent Cr zoning are from submarine lavas where the ratio Cr^{3+}/Cr^{2+} may be higher than those of samples from the Iki lava lake. Obviously, supposing an highest diffusivity of Cr^{2+} respect to that of Cr^{3+}, a predominance of Cr^{2+} would produce a Cr zoning more prone to be deleted. Combination of low Cr_2O_3 availability, longer exposure at high temperature, and predominance of Cr^{2+}, could have produced a very weak Cr zoning extremely difficult to be detected.

Phosphorous zoning and olivine growth

The observed P features are similar to those previously described both in natural and experimental olivines (Milman-Barris et al., 2008; Welsch et al., 2013, 2014; Shea et al., 2015; Bouvet de Maisonneuve et al., 2016; Neave et al., 2018), and the kinetics of crystal growth can be used to explain the complex zoning of P that is unrelated with zoning of divalent elements. These enrichments in P are due to the excessive incorporation of P during rapid growth. As P diffusivity in silicate melts is of the order of 10^{-11}-10^{-12} m^2/s (Baker, 2008; Watson et al., 2015), it is accumulated in boundary layers adjacent to rapidly growing crystals, and it is incorporated in olivine because of a disequilibrium partitioning coefficients value well above its equilibrium value. Phosphorous is also a slow diffusing element in olivine at magmatic temperature, being its diffusivity around 10^{-18} m^2/s at 1200 °C (Spandler et al., 2007; Watson et al., 2015). These properties permit to P zoning features in natural crystals to be accurately preserved over long timescales.

The equation of Albarede and Bottinga (1972) can characterize the kinetic disequilibrium of P between olivine and silicate melt due to the presence of a boundary layer in the melt. Assuming an infinite liquid reservoir, the temporal evolution of the concentration of a given trace element in a growing crystal (C^t_s) is given by equation (1). Equation (1) shows that the growth rate (G) of the crystal is too fast respect to the diffusivity of the trace element in the liquid to maintain an equilibrium condition between the crystal boundary and the far-field melt composition.

$$C^t_s/C_0 = 1/2K\cdot[1+erf(0.5(Gx'/D)^{0.5})+(2K-1)\cdot exp(-K(1-K)(Gx'/D)^{0.5})\cdot erfc(0.5(2K-1)(Gx'/D)^{0.5})] \quad (1)$$

Where C_0 is the initial, equilibrium trace element concentration in the solid, K is the partition coefficient crystal/melt, D is the diffusivity of the element in the melt, and x' is the half thickness of the crystal that started to grow at time zero. This equation shows that for a given amount of growth (x'), the excessive incorporation of nominally highly incompatible trace elements (C^t_s/C_0) rapidly increases with the rate at which the crystal grows (Bouvet de Maisonneuve et al., 2016).

Applying this model to olivine crystals of the Iki lava lake permits to evaluate the growth rates at which the high-phosphorous features were incorporated in olivine. The P contents of olivine crystals recovered from the different depths were normalized to the lowest, presumably equilibrium value, yielding an estimate of the magnitude of excessive incorporation (C^t_s/C_0; Figure 6). Partition coefficients are calculated from the data and are shown in Table 3. Diffusivity of elements in the melt are taken from Baker (2008), Zhang et al. (2010), and Watson et al. (2015). The high-P features are between 4 and 10 μm in width, with P contents that are factors of up to 60 higher than the non-zoned portions. Very high growth rate, in the range 10^{-5}-8×10^{-7} m/s, are predicted using the diffusivity data of Baker (2008), and even faster growth rates, in the range 10^{-4}-7×10^{-5} m/s, when using the diffusivity data of Watson et al. (2015).

When equation (1) is applied to Al and Ti rich-features accompanying P rich-layers, similar growth rates are estimated for Al, being in the range 10^{-5}-$7\cdot10^{-7}$ m/s, whereas Ti gives slower growth rate in the range $2\cdot10^{-6}$-$4\cdot10^{-8}$ m/s (Table 3). The lowest degree of enrichment (C^t_s/C_0) in Al and Ti is related to their faster diffusivity in olivine respect to P, which will cause their initial enrichments to decay with time respect to the well preserved P enrichments. Therefore, P together with Al and Ti register information about rapid growth events and have the potential to record the time elapsed since anomalous or disequilibrium concentrations were formed.

Information from olivine zoning

The X-ray maps and profile analyses of major and trace elements concentrations in several olivine grains recovered from different depths of the Iki lava lake show that, Fo, Ca, and Mn record only the events related to the crystals' thermal history (i.e., in this specific case their cooling), whereas elements such as P, Ti, and Al±Cr record the events related to the crystals' growth. Crystals from the shallow portion are normally zoned in Fo (Mg) with the intensity of the zoning decreasing with depth. The Fo zoning is accompanied by zoning in Ca and Mn, particularly evident in crystals from depth 45.3 and 55.2 m. No apparent zoning in divalent elements is found in crystals recovered from greater depths. These features suggest that zoning in divalent elements was driven by the different cooling history of the samples as a function of their position (i.e., depth) inside the lava lake and that is better preserved in the crystals that have experienced the lower residence temperature coupled to the highest degree of undercooling (expressed as the difference between the liquidus temperature of olivine and the temperature of the sample, i.e., quenching temperature, at the time of its recovery) and cooling rates (expressed as the degree of cooling per unity of time, °C/*t*). High degrees of undercooling associated with high cooling rates promote the formation and development of strong zoning in divalent elements, whereas low residence temperatures permit these zoning to be preserved for longer time respect to higher residence temperatures. The temperature profile (Figure 4) shows that the shallower samples, above 63.7 m, are those who had experienced the highest degree of undercooling and also the highest degree of cooling rate given the surface of the lava lake cooled in air whereas its bottom was in contact with rock and consequently the heat loss was less efficient (lower degree of undercooling and cooling rate respect to the shallower depths). Interestingly, the samples recovered at intermediate depths (63.7-78.0 m), being trapped between two layers of hot crystal mush, shows the highest quench temperatures and a limited temperature variability (only 6 °C) when compared to shallower (83 °C) and deeper samples (38 °C). Crystals from intermediate depths are those who experienced the lower degree of undercooling and cooling rates but the highest residence temperatures, consequently their zoning in divalent elements was fainter than those observed in shallower crystals and easily re-homogenized with time. Zoning in divalent elements is also absent in crystals recovered from the deeper section despite the temperature at the time of drilling for some of these samples is comparable to the quench temperature of the shallower samples. Given that these samples lie between a tick layer of hot magma at their top and a layer of country rock, relatively cold, at their bottom, it could be supposed they have experienced an undercooling and cooling rate intermediate respect to samples of the shallow and intermediate levels. All samples from this deepest section have quench temperatures similar or lower to that of samples from depth 60.3 m (i.e., the deepest samples still preserving zoning in divalent elements) but no residual zoning in Fo, Ca, and Mn. In particular, sample from depth 93.6 m (i.e., the deepest) has a quench temperature between those of samples 57.0 and 60.3 m but no residual zoning. Probably the undercooling itself was powerful enough to generate a strong zoning but it was buffered by the relatively low cooling rates these samples experienced, resulting in a final zoning that was weaker than expected and that was erased by their residence temperature.

The pattern of P zoning in olivines is complex and show various shapes, including P-rich zones as skeletal core sometimes surrounding melt inclusion, or as concentric and oscillatory regions inside the crystals separated by low-P zones. Similar patterns have already been reported elsewhere (Milman-Barris et al., 2008; Sakyi et al., 2012; Welsch et al., 2013, 2014; Neave et al., 2018). As observed by Welsch et al. (2014) P-rich regions are composed of

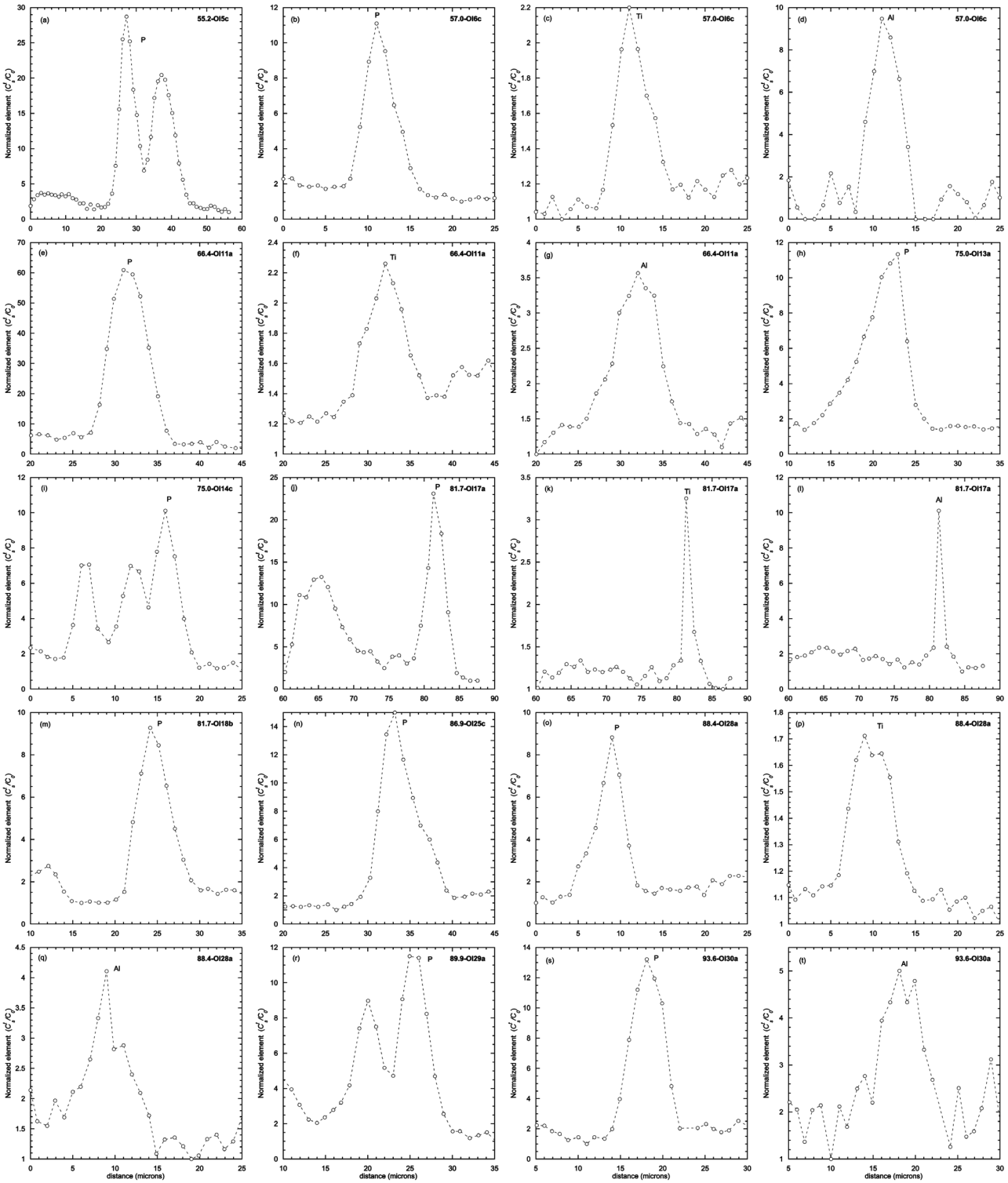

Figure 6. Enrichments of P, Al, ad Ti measured in olivine crystals as a function of distance (a-t). These excess were calculated by normalizing the concentration to the lowest, presumably equilibrium value.

Table 3. Parameters of the, kinetically controlled, enrichments of P, Ti, Al.

Sample	Element	C^t_s/C_0[a]	K[b]	D (m^2s^{-1})[c]	x'(μm)[d]	G (ms^{-1})[e]
55.2-Ol5c	P	28	1.3×10^{-2}	1.92×10^{-14}	8	2.8×10^{-6}
				6.95×10^{-13}*		1.0×10^{-4}
55.2-Ol5c	P	20	1.5×10^{-2}	1.92×10^{-14}	9.9	8.3×10^{-7}
				6.95×10^{-13}*		3.0×10^{-5}
57.0-Ol6c	P	11	1.5×10^{-2}	3.34×10^{-14}	5.5	6.4×10^{-7}
				9.83×10^{-13}*		1.9×10^{-5}
57.0-Ol6c	Ti	2.2	8.9×10^{-3}	4.82×10^{-13}	5.5	4.4×10^{-8}
57.0-Ol6c	Al	9.5	2.2×10^{-4}	2.53×10^{-13}	3.25	4.4×10^{-6}
66.4-Ol11a	Ti	2.3	6.6×10^{-3}	1.09×10^{-12}	5.5	1.1×10^{-7}
66.4-Ol11a	Al	3.6	9.4×10^{-4}	7.16×10^{-13}	6.5	2.7×10^{-7}
75.0-Ol14c	P	10	3.2×10^{-2}	8.47×10^{-14}	4	2.3×10^{-6}
				1.75×10^{-12}*		4.8×10^{-5}
75.0-Ol13a	P	11	2.4×10^{-2}	8.47×10^{-14}	7.5	1.5×10^{-6}
				1.75×10^{-12}*		3.0×10^{-5}
81.7-Ol18b	P	9.3	2.9×10^{-2}	7.83×10^{-14}	5	1.3×10^{-6}
				1.66×10^{-12}*		2.7×10^{-5}
81.7-Ol17a	P	23	2.3×10^{-2}	7.83×10^{-14}	5	1.6×10^{-5}
				1.66×10^{-12}*		3.3×10^{-4}
81.7-Ol17a	P	13	2.3×10^{-2}	7.83×10^{-14}	5	3.1×10^{-6}
				1.66×10^{-12}*		6.6×10^{-5}
81.7-Ol17a	Ti	3.3	8.6×10^{-3}	1.01×10^{-12}	1	1.9×10^{-6}
81.7-Ol17a	Al	10	1.4×10^{-3}	6.46×10^{-13}	3	1.5×10^{-5}
86.9-Ol25c	P	15	3.0×10^{-2}	6.77×10^{-14}	7	3.3×10^{-6}
				1.52×10^{-12}*		7.3×10^{-5}
88.4-Ol28a	P	8.8	2.3×10^{-2}	5.66×10^{-14}	5	7.3×10^{-7}
				1.36×10^{-12}*		1.8×10^{-5}
88.4-Ol28a	Ti	1.7	6.3×10^{-3}	7.61×10^{-13}	5	2.7×10^{-8}
88.4-Ol28a	Al	4.1	5.0×10^{-4}	4.53×10^{-13}	5	3.7×10^{-7}
89.9-Ol29a	P	12	1.7×10^{-2}	5.58×10^{-14}	5	1.4×10^{-6}
				1.35×10^{-12}*		3.3×10^{-5}
93.6-Ol30a	P	13	1.1×10^{-2}	4.25×10^{-14}	4	1.6×10^{-6}
				1.14×10^{-12}*		4.4×10^{-5}
93.6-Ol30a	Al	5.0	3.3×10^{-4}	3.29×10^{-13}	4	7.0×10^{-7}

[a]Excessive enrichment of nominally highly incompatible trace elements. [b]Partition coefficient crystal/melt. [c]Diffusivity values calculated combining the equations of Baker (2008) and Watson et al. (2015) for P and those of Zhang et al. (2010) for Ti and Al with the estimated quenching temperatures for glass compositions (supplementary material) calculated by the equation of Helz and Thornber (1987). *Phosphorous diffusivity values calculated by the equation of Watson et al. (2015). [d]width of the enriched zone. [e]Estimated growth rate by equation (1).

thin lineations located at the outer edges, medial regions, and center of crystals, and are oriented dominantly parallel to external faces (Figures S1-S5). Whereas in other crystals the P-rich lineations seem to propagate obliquely to external face, because these sections cut at an oblique angle the crystallographic axes (Welsch et al., 2014). These lineations are particularly evident in Figure S1 (63.7-Ol9B, 75.0-Ol13A, 86.9-Ol23), Figure S2 (45.3-

Ol2, 55.2-Ol3), Figure S3 (57.0-Ol6, 75.0-Ol14). All the P enriched lineations can be interpreted as the result of a dendritic growth, where the branches of the lineations emanate from the center of the crystal growing similarly to snowflakes (Welsch et al., 2014). Consequently, the particular shape of P lineations depends on the cutting angle between the sections and the crystallographic axes other than on the distance of the cut from the center of the crystal (Welsch et al., 2014). The main implication of the dendritic growth is that crystals do not develop a concentric pattern core-to-rim, where the layers are added to crystals sequentially from the older to the younger (Welsch et al., 2014). Instead, the more external P-rich lineations are believed to represent the oldest part of the crystals developed in a regime of fast growth, up to 10^{-6} m/s (Jambon et al., 1992), driven by the degree of undercooling and cooling rate (Welsch et al., 2013, 2014), followed by a subsequent event of growth at slower rate, 10^{-9} m/s (Jambon et al., 1992), that would define the final shape of the crystal and would develop the P-poor regions (Welsch et al., 2014). This implies that a 0.5 mm olivine would require only 8 minutes to crystallize and entrap P and other slow diffusing elements to develop the related zoning. The growth rates estimated from the high-phosphorous features confirm that the growth of olivine under conditions far from equilibrium, i.e., the growth process is diffusion controlled (Faure et al., 2007), is a very fast process of the order of minutes. On the other side, the overgrowths poor in P form at slower rate over a few weeks, yielding the final euhedral shape to the crystals. The rounded olivines present at different depths in the Iki lava lake, such as those in Figure S3 (57.0-Ol6, 63.7-Ol10, 66.4-Ol11b,c, 75.0-Ol15, 81.7-Ol18, 83.8-Ol19-20-21-22, 86.9-Ol26-27), are witnesses of the fast-growth process given they would have acquired a properly euhedral shapes, had these crystals continued to grow in a regime of slower growth (Welsch et al., 2014). Also the presence of melt and Cr-spinel inclusions, in various olivines of the Iki lava lake, near P-rich zones, (Figures S1-S6), strengthen the idea they were entrapped during a period of dendritic growth followed by a period of slower growth (Welsch et al., 2013, 2014).

Given that P zoning has been found also in plutonic olivines such as those from gabbros of the Mid-Atlantic Ridge and the Rum intrusion (Welsch et al., 2014) and in olivines from spinel peridotite (Mallman et al., 2009) is not astonishing to find this kind of zoning, testifying the presence of very fast dendritic growth processes driven by rapid cooling, in a lava lake only 135 m deep at its center (Helz, 2009). The rapid process of crystal growth inside the Iki lava lake may have been driven by heat transfer to the air and to the country rock. The weaker P zoning and the general absence of Cr and Al zoning in olivines from the Iki lava lake with respect to experimental charges (Milman-Barris et al., 2008; Welsch et al., 2014) or to rapidly cooled natural samples (e.g., pillow basalts, subaerial lava flows (Milman-Barris et al., 2008; Tschegg et al., 2010; Sakyi et al., 2012; Welsch et al., 2013, 2014) can be explained by the faster diffusion of Al and Cr respect to P (Ito and Ganguly, 2006; Spandler and O'Neill, 2010; Watson et al., 2015) and/or by their longer stay at magmatic temperatures.

CONCLUSIONS

The acquisition of a number of X-ray maps and line profiles of elements with different concentrations and geochemical properties in olivine crystals recovered from different depth inside the Kilauea Iki lava lake provides the possibility to interpret the magmatic processes operating during the cooling and crystallization of the lava lake. Divalent elements such as Ni, Mn and Ca can be related to Fo contents that together the residual concentric zoning in Mn and Ca were provoked by cooling of the lava lake for heat loss to air and/or to wall rocks. The absence of reverse zoning and resorption features in olivines tend to exclude the presence of events of magma mixing between the magma body of the lake and some mafic recharge. Trace elements such as Al, Cr, and Ti follow P for creating skeletal enrichments in olivines caused by kinetic disequilibrium partitioning during rapid crystal growth also caused by the cooling of the lava lake. All the above observations support the idea that the Kilauea Iki lava lake could be viewed as approaching closely an ideal closed system where its continuous and linear cooling provoked both the fast crystallization of olivines, recorded by P zoning and related elements, and their simple and normal zoning recorded by the divalent elements.

ACKNOWLEDGEMENTS

This article is the conclusion of a never ending work I started when I was a postdoctoral scholar at Caltech under the guidance of Ed Stolper. I wish to thank Ed for having amplified my curiosity for the unknown and for having pushed me to look at the scientific problem from a different perspective. Mike Baker and John Beckett are thanked for their tips and suggestions during my stay in Caltech. Ma Chi is thanked for his assistance at the electron microprobe and the Smithsonian Institution for providing samples. Federico Casetta is thanked for providing the official revision. I wish to send a special thought to Shelsy Diaz, a girl I had the privilege to crazy love. This work was supported by the Czech Science Foundation (project 18-01982S).

APPENDIX

Supplemental material and Deposited Item are available for downloading at the journal site.

REFERENCES

Albarède F. and Bottinga Y., 1972. Kinetic disequilibrium in trace-element partitioning between phenocrysts and host lava. Geochimica et Cosmochimica Acta 36, 141-156.

Armstrong J.T., 1988. Quantitative analysis of silicate and oxide minerals: Comparison of Monte Carlo, ZAF and $\phi(\rho z)$ procedures. In: Microbeam analysis. (Ed.): D.E. Newbury, San Francisco Press, San Francisco, 239-246.

Baker D.R., 2008. The fidelity of melt inclusions as records of melt composition. Contributions to Mineralogy and Petrology 156, 377-395.

Beattie P., 1994. Systematics and energetics of trace-element partitioning between olivine and silicate melts: Implications for the nature of mineral/melt partitioning. Chemical Geology 117, 57-71.

Berry A.J. and O'Neill H.St.C., 2004. A XANES determination of the oxidation state of chromium in silicate glasses. American Mineralogist 89, 790-798.

Berry A.J., O'Neill H.St.C., Scott D.R., Foran G.J., Shelley J.M.G., 2006. The effect of composition on Cr^{2+}/Cr^{3+} in silicate melts. American Mineralogist 91, 1901-1908.

Berry A.J., Walker A.M., Hermann J., O'Neill H.St.C., Foran G.J., Gale J.D., 2007. Titanium substitution mechanisms in forsterite. Chemical Geology 242, 176-186.

Blundy J. and Wood B., 2003. Mineral-melt partitioning of Uranium, Thorium and their daughters. In: Uranium-series geochemistry. (Eds.): B. Bourdon, G.H. Henderson, C.C. Lundstrom, S.P. Turner, Reviews in Mineralogy and Geochemistry 52, 59-123.

Bouvet de Maisonneuve C., Costa F., Huber C., Vonlanthen P., Bachmann O., Dungan M.A., 2016. How do olivines record magmatic events? Insights from major and trace element zoning. Contributions to Mineralogy and Petrology 171, 56, doi 10.1007/s00410-016-1264-6.

Byers C., Garcia M., Muenow D., 1985. Volatiles in pillow rim glasses from Loihi and Kilauea volcanoes. Geochimica et Cosmochimica Acta 49, 1887-1896.

Carmichael I.S.E., 1991. The redox state of a basic magma and silicic magmas: A reflection of their source region? Contributions to Mineralogy and Petrology 106, 129-141.

Carmichael I.S.E. and Ghiorso M.S., 1986. Oxidation-reduction relations in basic magma: A case for homogeneous equilibria. Earth and Planetary Science Letters 78, 200-210.

Dalton J.A. and Lane S.J., 1996. Electron microprobe analysis of Ca in olivine close to grain boundaries: The problem of secondary X-ray fluorescence. American Mineralogist 81, 194-201.

Dostal J., Dupuy C., Carron J.P., Dekerneizon M.L., Maury R.C. 1983. Partition coefficients of trace elements: application to volcanic rocks of St-Vincent, West-Indies. Geochimica et Cosmochimica Acta 47, 525-533.

Dunn T., 1987. Partitioning of Hf, Lu, Ti, and Mn between olivine, clinopyroxene and basaltic liquid. Contributions to Mineralogy and Petrology 96, 476-484.

Edmunson J., Borg L.E., Shearer C.K., Papike J.J., 2005. Defining mechanisms that disturb the Sm-Nd isotopic systematics of the Martian meteorites: examples from Dar al Gani 476 and Allan Hills 77005. Meteoritical Planetary Sciences 40, 1393-1411.

Faure F., Schiano P., Trolliard G., Nicollet C., Soulestin B., 2007. Textural evolution of polyhedral olivine experiencing rapid cooling rates. Contributions to Mineralogy and Petrology 153, 405-416.

Gaetani G.A. and Grove T.L., 1997. Partitioning of moderately siderophile elements among olivine, silicate melt, and sulfide melt: constraints on core formation in the Earth and Mars. Geochimica et Cosmochimica Acta 61, 1829-1846.

Helz R.T., 1987a. Diverse olivine types in lavas of the 1959 eruption of Kilauea Volcano, and their bearing on eruption dynamics. In: Volcanism in Hawaii. (Eds.): R.W. Decker, T.L. Wright, P.H. Stauffer, U.S. Geological Survey Professional Paper, 1350, 691-722.

Helz R.T., 1987b. Differentiation behavior of Kilauea Iki Lava Lake, Kilauea Volcano, Hawaii: an overview of past and current work. In: Magmatic Processes: Physicochemical Principles. (Ed.) B.O. Mysen, The Geochemical Society Special Publication 1, 241-258.

Helz R.T., 1993. Drilling report and core logs for the 1988 drilling of Kilauea Iki lava lake, Kilauea Volcano, Hawaii, with summary descriptions of the occurrence of foundered crust and fractures in the drill core. U.S. Geological Survey Open-file Report 93-13, 57 pp.

Helz R.T., 2009. Processes active in mafic magma chambers: The example of Kilauea Iki Lava Lake, Hawaii. Lithos 111, 37-46.

Helz R.T. and Thornber C.R., 1987. Geothermometry of Kilauea Iki lava lake, Hawaii. Bulletin of Volcanology 49, 651-668.

Ito M. and Ganguly J., 2006. Diffusion kinetics of Cr in olivine and Mn-53-Cr-53 thermochronology of early solar system objects. Geochimica et Cosmochimica Acta 70, 799-809.

Jambon A., Lussiez P., Clocchiatti R., 1992. Olivine growth rates in a tholeiitic basalt: An experimental study of melt inclusions in plagioclase. Chemical Geology 96, 277-287.

Jankovics M.E., Sagi T., Astbury R.L., Petrelli M., Kiss B., Ubide T., Nemeth K., Ntaflos T., Harangi S., 2019. Olivine major and trace element compsitions coupled with spinel chemistry to unravel the magmatic systems feeding monogenetic basaltic volcanoes. Journal of Volcanogy and Geothermal Research 369, 203-223.

Mallman G., O'Neill H.St.C., Klemme S., 2009. Heterogeneous distribution of phosphorous in olivine in otherwise well-equilibrated spinel peridotite xenoliths and its implications for the mantle geochemistry of lithium. Contributions to Mineralogy and Petrology 158, doi: 10.1007/s00410-009-0393-6.

Matzen A.K., Baker M.B., Beckett J.R., Stolper E.M., 2013. The

temperature and pressure dependence of Nickel partitioning between olivine and silicate melt. Journal of Petrology 54, 2521-2545.

Matzen A.K., Baker M.B., Beckett J.R., Wood B.J., Stolper E.M., 2017. The effect of liquid composition on the partitioning of Ni between olivine and silicate melt. Contributions to Mineralogy and Petrology 172, doi: 10.1007/s00410-016-1319-8.

Milman-Barris M.S., Beckett J.R., Baker M.B., Hofmann A.E., Morgan Z., Crowley M.R., Vielzeuf D., Stolper E., 2008. Zoning of phosphorus in igneous olivine. Contributions to Mineralogy and Petrology 155, 739-765.

Murata K.J. and Richter D.H., 1966. Chemistry of the lavas of the 1959-60 eruption of Kilauea Volcano, Hawaii. U.S. Geological Survey Professional Paper, 537-A, 26 pp.

Neave D.A., Shorttle O., Oeser M., Weyer S., Kobayashi K., 2018. Mantle-derived trace element variability in olivines and their melt inclusions. Earth and Planetary Science Letters 483, 90-104.

Potts P.J., 1987. A handbook of silicate rock analysis. Chapman and Hall, New York, 622 pp.

Poustovetov A.A. and Roeder P.L., 2001. The distribution of Cr between basaltic melt and chromian spinel as an oxygen geobarometer. The Canadian Mineralogist 39, 309-317.

Richter D.H. and Moore J.G., 1966. Petrology of the Kilauea Iki Lava lake, Hawaii. U.S. Geological Survey Professional Paper 537-B, 26 pp.

Richter D.H., Eaton J.P., Murata J., Ault W.U., Krivoy H.L., 1979. Chronological narrative of the 1959-60 eruption of Kilauea Volcano, Hawaii. U.S. Geological Survey Professional Paper 537-E, 73 pp.

Rhodes J.M. and Vollinger M.J., 2005. Ferric/ferrous ratios in 1984 Mauna Loa lavas: a contribution to understanding the oxidation state of Hawaiian magmas. Contributions to Mineralogy and Petrology 149, 666-674.

Roeder P.L., Thornber C., Poustovetov A., Grant A., 2003. Morphology and compsition of spinel in Pu'u 'O'o lava (1996-1998), Kilauea volcano, Hawaii. Journal of Volcanology and Geothermal Research 123, 245-265.

Roeder P.L. and Reynolds I., 1991. Crystallization of chromite and chromiumn solubility in basaltic melts. Journal of Petrology 32-5, 909-934.

Sakyi P.A., Tanaka R., Kobayashi K., Nakamura E., 2012. Inherited Pb isotopic records in olivine antecryst-hosted melt inclusions from Hawaiian lavas. Geochimica et Cosmochimica Acta 95, 169-195.

Scowen P.A.H., Roeder P.L., Heltz R.T., 1991. Reequilibration of chromite from Kilauea Iki lava lake, Hawaii. Contributions to Mineralogy and Petrology 107, 8-20.

Shannon R.D., 1976. Revised effective ionic redii and systematic studies of interatomic distances in halides and chalcogenides. Acta Crystallographica A32, 751-767.

Shea T., Lynn K.J., Garcia M.O., 2015, Cracking the olivine zoning code: distinguishing between crystal growth and diffusion. Geology 43, 935-938.

Spandler C. and O'Neill H.St.C., 2010. Diffusion and partition coefficient of minor and trace elements in San Carlos olivine at 1300 °C with some geochemical implications. Contributions to Mineralogy and Petrology 159, 791-818.

Spandler C., O'Neill H.St.C., Kamenetsky V.S., 2007. Survival times of anomalous melt inclusions from element diffusion in olivine and chromite. Nature 447, 303-306.

Teng F.-Z., Dauphas N., Helz R.T., 2008. Iron isotope fractionation during magmatic differentiation in Kilauea Iki lava Lake. Science 320, 1620-1622.

Tschegg C., Ntaflos T., Kiraly F., Harangi S., 2010. High temperature corrosion of olivine phenocrysts in Pliocene basalts from Banat, Romania. Australian Journal of Earth Science 103, 101-110.

Villemant B., 1988. Trace-element evolution in the phlegrean fields (Central-Italy): fractional crystallization and selective enrichment. Contributions to Mineralogy and Petrology 98, 169-183.

Watson E.B., 1977. Partitioning of manganese between forsterite and silicate liquid. Geochimica et Cosmochimica Acta 41, 1363-1374.

Watson E.B., Cherniak D.J., Holycross M.E., 2015. Diffusion of phosphorous in olivine and molten basalt. American Mineralogist 100, 2053-2065.

Welsch B., Faure F., Famin V., Baronnet A., Bachèlery P., 2013. Dendritic crystallization: a single process for all the textures of olivine in basalts? Journal of Petrology 54, 539-574.

Welsch B., Hammer J.E., Hellebrand E., 2014. Phosphorus zoning reveals dendritic architecture of olivine. Geology 42, 867-870.

Wright T.L., 1973. Magma mixing as illustrated by the 1959 eruption, Kilauea Volcano, Hawaii. Geological Society of America Bulletin 84, 849-858.

Zhang Y.X., Ni H.W., Chen Y., 2010. Diffusion data in silicate melts. In: Diffusion in minerals and melts. (Eds.): Y. Zhang and D.J. Cherniak, Reviews in Mineralogy and Geochemistry 72, 311-408.